# A Three-Dimensional Inertial Model for Coastal Upwelling

Haihong Guo*[1,2,3], Michael A. Spall[3], Joseph Pedlosky[3], Zhaohui Chen[1,2]

[1]Key Laboratory of Physical Oceanography/Institute for Advanced Ocean Science/Frontiers Science Center for Deep Ocean Multispheres and Earth System, Ocean University of China, Qingdao, China

[2]Pilot National Laboratory for Marine Science and Technology (Qingdao), Qingdao, China

[3]Department of Physical Oceanography, Woods Hole Oceanographic Institution, Woods Hole, MA, USA

[*] *Corresponding author*: Haihong Guo guohaihong@stu.ouc.edu.cn

Physical Oceanography Laboratory, Ocean University of China, 238 Songling Road, Qingdao 266100, China.

## Abstract

A three-dimensional inertial model that conserves quasigeostrophic potential vorticity is proposed for wind-driven coastal upwelling. The dominant response to upwelling favorable winds is a surface intensified baroclinic meridional boundary current with a subsurface countercurrent. The width of the current scales with the inertial boundary layer thickness and the depth scales as the ratio of the inertial boundary layer thickness to the baroclinic deformation radius and thus depends on the stratification, wind stress, Coriolis parameter, and its meridional variation. In contrast to two-dimensional wind-driven coastal upwelling, the source waters that feed the Ekman upwelling are provided over the depth scale of this baroclinic current through a combination of onshore barotropic flow and from alongshore in the narrow boundary current. Topography forces an additional current whose characteristics depend on the topographic slope and width. For topography wider than the inertial boundary layer thickness the current is bottom intensified while for narrow topography the current is wave-like in the vertical and trapped over the topography within the inertial boundary layer. An idealized primitive equation numerical model produces a similar baroclinic boundary current whose vertical length scale agrees with the theoretical scaling for both upwelling and downwelling favorable winds.

## 1 Introduction

Wind-driven upwelling and downwelling are key processes in the coastal ocean circulation that connect the surface and interior ocean. The onshore/offshore Ekman transport in the surface layer provides downwelling/upwelling, which is supplied by a combination of offshore/onshore return flow below the Ekman layer and flow along the boundary. These processes play important roles not only in the water exchange between the surface Ekman layer and interior but also in the primary production and chlorophyll redistribution (Hickey, 1998).

The wind-driven coastal upwelling theory has been studied in many works. The upwelling can bring deep isopycnals to the upper layer, resulting in sloping isopycnals over a horizontal scale of the baroclinic deformations radius (Charney 1955), which builds an alongshore, geostrophic flow. Using a two-dimensional, non-dissipative, nonlinear model, Pedlosky (1978) showed a sharp gradient on scales much less than the Rossby deformation radius was forced by coastal upwelling, which can be observed to form during the initiation of upwelling (Halpern, 1974). In the time-dependent, two-dimensional model of Choboter et al. (2005), an equatorward boundary current develops more rapidly in the upper ocean followed by a deeper poleward undercurrent. There is a near-surface offshore flux of faster alongshore flow and an onshore flux of slower alongshore flow throughout the interior. Compared to the flat bottom ocean, the cross-shore topography plays an important role in the cross-slope flow and the along-slope baroclinic flow. The cross-slope flow is slow and surface intensified over steep slopes, while the along-slope velocity has a strong vertical dependence and develops an undercurrent (Choboter et al. 2011), and vice versa for shallow slopes. The partition between onshore flow in a bottom Ekman layer and onshore flow in the interior depends on the slope Burger number (Lentz and Chapman, 2004). When the Burger number is small (weak stratification) the onshore flow is carried in a bottom Ekman layer and the wind stress is balanced by bottom stress. However, when the Burger number is large (strong stratification or steep slope) the onshore flow is carried in the interior and the cross-shelf momentum flux divergence balances the wind stress.

However, these studies are two-dimensional in the depth-offshore plane and thus require that the offshore Ekman transport be balanced by onshore flow below the Ekman layer, either in the interior or in a viscous bottom boundary layer. However, if the wind-forcing is spatially variable in the along-coast direction the flow will be three dimensional. This introduces a potential source to balance the offshore Ekman transport from along the boundary. Using A two-layer model with an idealized continental shelf and slope bottom topography, Allen (1976) showed that the alongshore and time-dependent behavior the baroclinic and barotropic components are governed by forced continental Kelvin waves. Therefore, the region of forced upward motion of density surfaces may propagate alongshore to locations distant from that of the wind stress, which results in the set-up of alongshore barotropic currents at locations in the down-wave direction of the wind stress that forces them. Yoon and Philander (1982) demonstrated that baroclinic Kelvin waves excited by the onset of winds that adjust the pressure field arrest the acceleration of the coastal jet and the upwelling. Meanwhile, a coastal undercurrent is established by the difference between the vertical structure of the waves and the coastal jet.

We are interested in the magnitude and three-dimensional structure of currents forced by coastal upwelling and downwelling. In particular, we are interested in what controls the depth from which the offshore Ekman transport draws fluid from the interior and in the partition between interior and boundary sources. Motivated by a recent work about the interaction of the Ekman layer and island boundary (Pedlosky, 2013), the theory is developed for steady, adiabatic, inviscid quasigeostrophic fluid over a sloping bottom. Comparisons with an idealized primitive equation model support the basic conclusions drawn from the steady quasigeostrophic theory.

## 2 Theory

### *a. Equations*

We consider a non-linear model for the steady-state circulation in a uniformly stratified ocean, with bottom topography declining in the cross-shore direction from an elevation $h^*$ at the western boundary. The model is adiabatic and inviscid and conserves quasigeostrophic potential vorticity. In order to most clearly expose the parameter sensitivity and the structure of the circulation forced by the interaction of the Ekman transport with a boundary, we consider the nondimensional form of the equations. The vertical coordinate is scaled by the ocean depth far from the western boundary, $H^*$, and the horizontal length is scaled by $L^*$, which could be chosen to be the deformation radius. All variables with an asterisk are dimensional, and henceforth those lacking an asterisk are nondimensional.

The flow is driven by a uniform northward wind stress on a beta-plane, therefore, a nearly meridionally uniform zonal transport within the Ekman layer is drawn away from the western boundary. The wind stress is uniform and has no curl so that there is no Ekman pumping in the interior, allowing us to focus on the interaction between the Ekman layer and western boundary. It is suggested that the offshore Ekman flux is balanced by the interior geostrophic flow. Therefore, we set the eastern boundary condition below the Ekman layer as a uniform, barotropic, geostrophic zonal westward flow far from the western boundary with magnitude $U^* = \tau^* / \rho_0 f_0 H^*$, where $f_0$ is the dimensional Coriolis parameter at the meridional center of the model domain, and $\rho_0$ is the mean density in the Boussinesq approximation. Although the discussion is framed for a western boundary with coastal upwelling, the same approach could be applied to an eastern boundary with coastal downwelling.

Following Pedlosky (2013), the nondimensional quasigeostrophic potential vorticity is defined as

$$q = \nabla^2 \psi + \frac{1}{S}\frac{\partial^2 \psi}{\partial z^2} + by \quad (1)$$

where $b = \beta L^{*2} / U^*$ and $S = N^2 H^{*2} / f_0^2 L^{*2}$, $\beta$ is the dimensional planetary vorticity gradient and $N$ is the uniform buoyancy frequency.

The potential vorticity is a constant along streamlines for steady adiabatic, frictionless flow. Far from the western boundary, the potential vorticity is simply specified by the latitude at which the flow enters the domain

$$q = by = \frac{b}{U}\psi = Q(\psi) \quad (2)$$

Since $q$ is conserved following the flow, the potential vorticity is a function of the streamfunction. This relationship will continue to hold on all streamlines as they approach the western boundary.

The vertical boundary conditions require that the normal component of the velocity at the surface and the bottom be zero. Following Pedlosky (2013), the vertical velocity required at the bottom is given by

$$w = \mathbf{u} \cdot \nabla h = J(\psi, h) = -\frac{1}{S} J\left(\psi, \frac{\partial \psi}{\partial z}\right), \quad z = 0 \quad (3)$$

where $h = \left(f_0 h^* / H^* U^*\right) L^*$ is the nondimensional topographic height. Because the flow is adiabatic, the vertical velocity can also be related to the horizontal advection of the perturbation density and the stratification, which gives rise to the equality on the right hand side. Consistent with the quasigeostrophic approximation, this boundary condition is applied at $z = 0$. Since both

$\partial\psi/\partial z$ and $h$ are zero far from the western boundary, if we integrate (3) far from the boundary to an arbitrary position over the topography, $h+\frac{1}{s}\partial\psi/\partial z$ must vanish. Therefore, the bottom boundary condition becomes

$$\frac{\partial\psi}{\partial z}=-Sh, \quad z=0 \ (4)$$

On the upper boundary,

$$\frac{\partial\psi}{\partial z}=0, \quad z=1 \ (5)$$

The topography decays in the zonal direction from $h_0$ at the western boundary to zero over a horizontal e-folding length scale $\lambda$,

$$h=h_0e^{-\lambda x} \ (6)$$

The lateral boundary condition at the western boundary is related to the Ekman flux. The Ekman layer is extremely thin compare to the total depth and is non-divergent except at the western boundary. We assume that the Ekman layer lies outside our model domain and acts as a boundary condition at $x=0,\ z=1$. Therefore, we use a Dirac function to represent this source at the western boundary. That is

$$u=-\frac{\partial\psi}{\partial y}=-U\delta(z-1), \quad x=0 \ (7)$$

so that the zonal velocity is zero at the western boundary below the surface and of sufficient strength at the surface to draw fluid from below to balance the offshore Ekman transport.

The full equations for the interior ocean below the Ekman layer are then

$$q=\nabla^2\psi+\frac{1}{S}\frac{\partial^2\psi}{\partial z^2}+by=\frac{b}{U}\psi \ (8a)$$

$$\frac{\partial \psi}{\partial z} = -Sh, \quad z = 0 \quad (8b)$$

$$\frac{\partial \psi}{\partial z} = 0, \quad z = 1 \quad (8c)$$

$$\frac{\partial \psi}{\partial y} = U\delta(z-1), \quad x = 0 \quad (8d)$$

*b. Solutions*

To solve these equations, we first write

$$\psi = Uy + \varphi \quad (9)$$

where $\varphi$ is the perturbation streamfunction representing the adjustment of the interior geostrophic pressure due to the presence of the boundary and the sink at the corner. Therefore, $\varphi$ satisfies

$$\frac{\partial^2 \varphi}{\partial x^2} + \frac{1}{S}\frac{\partial^2 \varphi}{\partial z^2} - \frac{b}{U}\varphi = 0 \quad (10a)$$

$$\frac{\partial \varphi}{\partial z} = -Sh, \quad z = 0 \quad (10b)$$

$$\frac{\partial \varphi}{\partial z} = 0, \quad z = 1 \quad (10c)$$

$$\varphi = (Uy - \psi_0)[\delta(z-1) - 1], \quad x = 0 \quad (10d)$$

where $\psi_0$ is the pressure on the boundary which determines the position of the stagnation point and we are free to specify as a boundary condition.

Anticipating a boundary layer structure, the alongshore scale is assumed to be much greater than the cross-shore scale, therefore, in (10a) derivatives in the *y*-direction have been dropped.

A particular solution of (10a), which satisfies the vertical boundary condition (10b, c) is,

$$\varphi_p = h_0 \frac{S}{m} e^{-\lambda x} \frac{\cosh m(z-1)}{\sinh(m)} \quad (11a)$$

$$m = S^{1/2} \sqrt{\frac{b}{U} - \lambda^2} \quad (11b)$$

This particular solution only satisfies the vertical boundary conditions so homogenous solutions are needed to match the lateral boundary conditions.

The lateral condition at western boundary, rewritten in terms of perturbation streamfunction, is then

$$Uy - \psi_0 + \varphi_p + \varphi_h = \left(Uy - \psi_0\right)\delta(z-1), \quad x = 0 \quad (12)$$

It is clear that the homogeneous component contains two independent solutions, the source/sink solution forced by interaction between the zonal flow and the bottom topography and the Ekman pumping/sucking at the corner. These solutions will be labeled $\varphi_h^0$ and $\varphi_h^1$, respectively.

It follows directly that the source/sink solution is

$$\varphi_h^1 = \sum_{n=1}^{+\infty} 2\left(Uy - \psi_0\right) e^{-\alpha x} (-1)^n \cos(n\pi z) \quad (13a)$$

$$\alpha^2 = \frac{b}{U} + \frac{n^2\pi^2}{S} \quad (13b)$$

Note that the source/sink solution has no barotropic component, which is not surprising because the vertical integral of the first two terms on the left side of (12) is equal to the integral of the right hand side.

The homogeneous topographic forced solution is

$$\varphi_h^0 = \sum_{n=0}^{\infty} A_n e^{-\alpha x} \cos(n\pi z) \quad (14)$$

Since the source/sink solution has already satisfied the geostrophic lateral boundary condition, more conditions are required to determine the topographic solution. Consider the linear meridional momentum equation adjacent to the boundary with a small artificial friction proportional to the meridional velocity $v$, where $\varepsilon = 1$,

$$\frac{\partial v}{\partial t} + f_0 u_a = -\varepsilon v \quad (15)$$

For a steady flow, since the homogeneous topographic solution is independent of $y$ and thus has no zonal geostrophic component, the balance is between friction and the ageostrophic zonal velocity $u_a$. Since the velocity normal to the boundary must be zero at $x = 0$, this requires that $v = 0$ even in the limit of vanishing $\varepsilon$. Therefore, the along-shore velocity $v$ is set to zero for the topographic solutions, from which it follows

$$\frac{d\varphi_h^0}{dx} + \frac{d\varphi_p}{dx} = 0, \quad x = 0 \quad (16)$$

Applying (12) and (14) to (16) yields the homogeneous topographic solution

$$\varphi_h^0 = \sum_{n=0}^{\infty} -\frac{2\varepsilon_n h_0 S\lambda}{\alpha\left(\pi^2 n^2 + m^2\right)} e^{-\alpha x} \cos(n\pi z) \quad (17a)$$

$$\varepsilon_n = \begin{cases} \frac{1}{2}, & n = 0 \\ 1, & n \geq 1 \end{cases} \quad (17b)$$

**2. Discussion**

Although most of the analysis will be in nondimensional parameter space, it is helpful to frame the discussion at the outset by identifying the order of magnitude of the nondimensional numbers derived from typical oceanic parameters. Dimensional parameters representative of the mid-latitude oceans are: $\tau^* = 0.1\ \mathrm{kg\ m^{-1}\ s^{-2}}$, $\rho_0 = 10^3\ \mathrm{kg\ m^{-3}}$, $f_0 = 10^{-4}\ \mathrm{s^{-1}}$, $H^* = 10^3\ \mathrm{m}$,

$L^* = 10^5$ m, $\beta = 10^{-11}$ m$^{-1}$ s$^{-1}$. This results in an onshore barotropic velocity of $U^* = 10^{-3}$ m s$^{-1}$. Using these values, the nondimensional numbers scale as

$$U = O(1), \quad b = O\left(10^2\right), \quad S = O(1) \tag{18}$$

We set the parameters $S$ = 1, $U$ = 1, $b$ = 100, and $\lambda$ = 5 in the standard calculation. The sensitivity to these parameters will also be discussed.

*a. The boundary pressure* $\psi_0$

A representative solution for the streamfunction is shown in Fig. 1a, b at two depths, one averaged between $z$ = 0.8 and $z$ = 1.0 and the other near the bottom ($z$ = 0.1). For this choice of $\psi_0 = 5$, the flow is symmetric in the meridional direction about $y$ = 5. Deep in the water column, the interior flow approaches the western boundary and is diverted northward and southward in a narrow boundary layer. However, near the surface, the flow develops a narrow boundary current with increasing strength away from the $\psi_0$ streamline. The flow in the boundary current is directed towards the latitude $\psi_0$ from both the north and south, in the opposite direction to the deep flow. There is also a component of the flow directed towards the boundary. This provides the source waters that are drawn into the Ekman layer in the corner. The balance in the potential vorticity terms is between relative vorticity and stretching vorticity, variations in planetary vorticity are locally relatively unimportant.

The solution depends on the choice of $\psi_0$, the pressure on the boundary. A choice of $\psi_0 = 0$ would result in all of the deep onshore transport turning towards the north with a strong boundary current near the surface, as seen in Fig. 1b for $y$ > 5. It can be most easily understood by recognizing that the streamfunction holds as a constant line along the reference latitude far from the ocean interior to the boundary. Therefore, to the north/south of this latitude, the pressure at the boundary is smaller/larger than the ocean interior, which builds a northward/southward flow near the boundary. It can also be understood from the vorticity balance. Since we assume the ocean interior is frictionless, the vorticity balance of the deep circulation within the boundary layer is between the relative vorticity and planetary vorticity. Furthermore, the main component of the relative vorticity is attributable to the meridional velocity because in the boundary layer the zonal scale is much smaller than the meridional scale. Therefore, the deep impinging flow moves either northward or southward, which depends on the boundary condition that we choose at $x = 0$.

The value of $\psi_0$ is determined by processes outside the local region of wind forcing. The boundary pressure is propagated along the boundary by waves (Allen, 1976; Yoon and Philander, 1982). In the case of spatially limited wind stress, the boundary pressure at the upstream (in the wave phase speed sense) limit of the wind stress would determine $\psi_0$. In that case the flow in the boundary current would be from the south towards the latitude where the wind stress ceases, as in the two-layer solutions of Allen (1976). For example, in Fig. 1, if the wind were set to zero for $y > 5$ the solution for $y < 5$ would be unchanged. For the cases considered here, with spatially uniform wind stress in a closed basin, the boundary pressure would be determined by a contour integral around the whole basin, which would presumably involve distant wind forcing and dissipation. One can imagine a similar downwelling boundary layer on the eastern boundary that exports water to the south in a narrow boundary current that closes the circulation with this western boundary current. Although the flow direction depends on the boundary constant, the boundary layer width and vertical scale, the primary quantities of interest here, do not depend on $\psi_0$. Therefore, in the further analysis, we diagnose the boundary current structure at $y = 0$ without loss of generality.

*b. The total solution*

The total solution for the velocity shows that a southward meridional flow arises as the boundary is approached at all depths, with a stronger, narrower boundary current in the upper layers compared to the lower layers (Fig. 2a). An adjacent northward velocity develops in the upper ocean on the offshore side of this narrow flow. The deep meridional velocities have very weak vertical shear and are trapped near the western boundary with scale $L_I = \sqrt{U / b}$. This is the inertial boundary layer, which is governed by a potential vorticity balance between relative vorticity and the planetary vorticity gradient. The ratio of this inertial boundary layer width to the baroclinic deformation radius is given by $L_I / L_d = \sqrt{U / Sb}$ and, for the present parameters, is much less than one.

Pedlosky (2013) found similar results for the interaction of surface Ekman transport with an island, with some of the streamlines feeding the eastern upwelling directly from the interior and some from along the island perimeter. If the island radius in Pedlosky (2013) is much larger than the deformation radius, the streamlines around $y = 0$ are similar to our straight boundary solution.

The total solution contains three parts, the flat bottom source/sink forcing solution, the particular solution, and the topographic homogeneous solution. Because the problem is linear, we may consider each of these components separately.

*c. Flat bottom contribution*

The flat bottom source/sink solution is much stronger than the particular and homogeneous solutions forced by topography (Fig. 2b). For the barotropic part of the interior flow, the stretching vorticity is negligible because the height variations are small over a length scale less than the order of the deformation radius in the quasigeostrophic framework. The deep flow potential vorticity balance of the source/sink solution is mainly between the relative vorticity and planetary vorticity, which are the first and third term in (10a). Therefore, the streamfunction anomaly owing to the source/sink forcing is intensified at the western boundary, which decays eastward with the inertial boundary layer width. This is demonstrated in Fig. 3a in which the horizontal scale of the deep flow was diagnosed from a series of solutions with different values for $S$, $U$, $b$, and $\lambda$, as summarized in Table 1. The horizontal scale was diagnosed as the location of the e-folding of the boundary streamfunction anomaly at $z = 0.5$. The diagnosed boundary current width scales with $\sqrt{U/b}$ in Fig. 3a (solid line). This demonstrates that vortex stretching is negligible in the deep ocean and the balance is between relative vorticity and beta. Not surprisingly, the horizontal scale of the deep flow is not sensitive to $S$ (not shown).

The source/sink solution shows strong baroclinicity especially as the flow in the upper ocean enters into the inertial boundary layer. The streamfunction of the source/sink solution shows a sharper gradient in the upper layer than the lower layer (Fig. 1a, b). The delta function forcing at the surface results an intense, narrow structure, particularly as the surface is approached (Fig. 2b). The baroclinic structure shows a local maximum southward flow lying below the strong northward boundary current. However, if one averages in the vertical the net transport in this upper ocean baroclinic flow becomes evident (Fig. 1a). Below this the southward flow becomes independent of depth. The horizontal width of this baroclinic meridional boundary current scales as $1/\alpha$, which can be demonstrated from (13). The parameter scaling (18) shows that the typical value of the nondimensional number $b$ is much larger than $S$ and $U$. Therefore, in the series solution, $b/U > n^2\pi^2/S$ for small $n$. Meanwhile, the remaining terms play a decreasing role in the summation of the series solution as $n$ increases, especially for small $z$, owing to the cosine function. Therefore, the horizontal scale $1/\alpha$ can be approximated as $\sqrt{U/b}$ in the lower layers, consistent with Fig. 3a. However, as $z$ increases from 0 towards 1, the remaining terms are beginning to play a more important role even for large $n$ in the summation of the cosine series, resulting in the variability on a scale $1/\alpha < \sqrt{U/b}$, which means a sharper pressure gradient, and stronger currents, in the upper layer than in the lower layer.

The stretching vorticity starts to play an increasing role near the surface in the vorticity balance. Given that the stretching does not contribute to the barotropic vorticity and the baroclinic solution is surface intensified (Fig. 2b) for the source/sink solution in a flat bottom ocean, the streamfunction anomaly due to the baroclinic stretching is strong near the surface and decays with depth. The balance between the planetary vorticity and stretching vorticity in (10a) shows that the key parameter of the baroclinic current forced by the source/sink solution is $U/Sb$, which is the ratio of planetary vorticity to stretching vorticity as well as the ratio of the inertial boundary layer width and the deformation radius, squared. If $U/Sb =$ 1, the vertical length scale has to be small in order for the stretching term to balance the relative vorticity term. In the other limit, $U/Sb$ ? 1, the stratification is weak and the vertical length scale approaches the bottom depth. As the flow moves into the boundary layer, the relative vorticity starts playing an increasingly role in the potential vorticity balance. In the boundary layer $x < \sqrt{U/b}$, the relative vorticity in (10a) exceeds the planetary vorticity advection, which then requires a smaller vertical scale so that the stretching vorticity can adjust to conserve $q$.

The vertical scale was diagnosed as the depth of the e-folding of the surface streamfunction anomaly at $x = \sqrt{U/b}$. The vertical scale is plotted as a function of $\sqrt{U/Sb}$ in Fig. 3b (solid line), which is also well predicted by the theory, especially for small $\sqrt{U/Sb}$. Physically, the larger the wind strength means the stronger the onshore flow, which turns to the meridional flow in the boundary layer. In order to balance the same strength of planetary vorticity variation, the same relative vorticity forced by stronger onshore flow results in a larger horizontal scale for strong boundary flow. The vertical scale can also be understood from the balance between the relative vorticity and stretching vorticity in (10a), where the horizontal scale of the relative vorticity is the inertial boundary layer thickness $\sqrt{U/b}$. The vertical scale is obtained by taking the ratio of the first term for the second term in (10a). Therefore, the vertical scale depends on the horizontal scale through the vorticity balance in (10a), which is also larger for stronger wind stress. The stratification plays an important role in the stretching vorticity variation (10a). For weak/strong stratification, the stretching vorticity is also weak/strong, which needs a large/small vertical scale to balance vorticity variations. As the stratification tends to zero, the stretching vorticity is not effective and the solution becomes barotropic. The dependence of the scales on $b$ can be understood from recognizing that a stronger planetary vorticity gradient requires stronger relative vorticity and stretching vorticity, which means a narrower boundary layer thickness.

*d. The topographic contribution*

Topography enters the problem in two ways. First, it alters the flat bottom solution, that is, the stretching vorticity is involved in the barotropic vorticity balance over the topographic length scale $1/\lambda$. As the interior flow moves across the sloping topography it introduces stretching of planetary vorticity, $fw_z$, that tends to increase the potential vorticity, this is balanced by southward advection of planetary vorticity (Fig. 2c). Therefore, the horizontal scale of the stretching vorticity induced by topography depends on the topographic scale, which is distinct from the boundary layer thickness. As the flow impinges on the western boundary, the vorticity balance in the western boundary layer over topography is not only between relative vorticity and planetary vorticity, but the stretching vorticity is also active. Second, it provides a forcing at

$z = 0$ through the no-normal flow condition at the bottom. This supports a bottom-intensified baroclinic current that decays upward with an e-folding scale of $1/m$ (Fig. 3c).

The vertical structure of the particular solution depends on the topographic slope (11a, b). For wide topographic slopes ($\lambda^2 < b/U$), $m$ is real and the particular solution is a bottom-intensified flow over the slope, as in Fig. 2c. In this regime the topography is wider than the inertial boundary layer width, relative vorticity of the particular solution is small, and the potential vorticity balance is primarily between vertical stretching and advection of planetary vorticity. This is the most relevant regime for the mid-latitude ocean. The strength of the particular solution is far smaller than the source/sink solution and the vertical scale of the particular solution is always larger than the source/sink solution since $m < \sqrt{Sb/U}$ in this limit. Physically, the dependence of vertical scale on stratification, geostrophic flow strength, and $\beta$ is the same as the vertical scale of source/sink solution but trapped in the bottom layer.

If $\lambda^2 = b/U$, the topography is exactly the width of the inertial boundary layer and $m = 0$ so the balance is between relative vorticity and $\beta$ and the particular response is barotropic.

For topography narrower than this ($\lambda^2 > b/U$) $m$ becomes imaginary, which results in wave-like solutions in the vertical. In this limit the relative vorticity produced by the narrow topographically-induced flow is larger than can be balanced by advection of planetary vorticity and so the stretching term is required to balance. The stretching contribution is of opposite sign in this limit compared to the wide topography case.

The homogeneous topographic forced solution is a maximum at the western boundary and decays eastward with horizontal scale $1/\alpha$ (17a). Since the particular solution satisfies the vertical boundary condition and the topographic forcing solution is a supplemental solution that matches the lateral boundary condition, the topographic forced solution shares the same vertical scale with the particular solution.

The source/sink forcing solution has no barotropic component. However, for nonzero topography, the particular and topographic solutions do contain barotropic components (Fig. 4a, b). Both the particular and topographic solutions are boundary intensified but with different scales. The particular solution decays eastward with a scale depending on the topographic extension from the western boundary, while the homogenous topographic forcing solution decays over the inertial boundary layer width (the same decay scale as the source/sink solution), which is independent of the topography (Fig. 4b). The barotropic velocity over the topography increases as the width $(1/\lambda)$ decreases or the maximum height at the boundary $h_0$ increases. Although the streamfunction anomaly of the particular solution at the boundary depends only on $h_0$ (11), the decay of the streamfunction anomaly depends on the topographic scale $(1/\lambda)$, resulting in distinctive boundary currents with different topographic scales (Fig. 4a, b). The boundary perturbation streamfunction of the homogenous topographic solution is sensitive to both $h_0$ and $\lambda$. The velocity of the homogeneous topographic solution is reversed but with the same magnitude as the particular solution at the boundary. Therefore, the solutions forced by the topography have no meridional velocity at the western boundary, which is the no-slip boundary condition (16).

*e. The mass budgets*

These solutions provide a framework for understanding the mass budget and the origin of water that is drawn into the Ekman layer. The zonal flow approaching the western boundary is exactly that required to balance the offshore Ekman transport. However, the deep flow turns parallel to the boundary, it does not upwell into the Ekman layer. This is a major difference between these three-dimensional solutions and two-dimensional solutions (e.g. Lentz and Chapman, 2004; Choboter et al., 2011). So, the logical question is, if this deep water is not entering the Ekman layer, where does that transport into the Ekman layer come from?

The upper ocean streamfunction in Fig. 1a shows that the upwelling is provided by the meridional flow in the baroclinic boundary current, which feeds into a vanishingly thin boundary layer that ultimately feeds the upwelling into the Ekman layer. Additional physics that include mixing and viscosity, not considered here, would be required to explicitly represent the balances in this narrow boundary region. The depth that marks the transition between the deep recirculating flow and the source waters for the Ekman layer is the vertical length scale for the baroclinic flow, $L_I / L_d = \sqrt{U / Sb}$. Given that the perturbation solution has zero depth-integrated meridional transport, the meridional transport shallower than this depth is of equal magnitude and in the opposite direction to the deep flow and thus provides the transport required by the offshore Ekman flow. As the boundary is approached, the deep zonal flow approaches zero over a horizontal length scale $\sqrt{U / b}$. In order to keep the source/sink forced perturbation solution purely baroclinic, the upper layer zonal flow increases towards the boundary over this same length scale. Therefore, the water that gets upwelling into the Ekman layer comes primarily from the upper ocean shallower than $\sqrt{U / Sb}$ and is advected into the upwelling region through a combination of a meridional boundary current of the inertial boundary layer width and the onshore flow in the interior. The direction of the meridional flow that supplies the source waters in the baroclinic boundary current depends on the choice of boundary constant $\psi_0$. This means that the depth of the source waters that feed Ekman upwelling is not an inherent length scale that depends only on the local environmental parameters but instead deepens as the wind forcing strengthens, as the stratification weakens, or as the Coriolis parameter increases. In dimensional units, this vertical length scale is $D = f_0 / N\sqrt{U^* / \beta}$ which, for typical parameter, is $O$(100 m).

This also provides a scaling for the magnitude of the meridional velocity in the boundary current since it has to provide the transport into the Ekman layer that is not provided from the interior onshore flow. If one takes the deep southward transport, which scales as $U(1-\sqrt{U/Sb})L_y$, and requires that this be provided in a boundary current of horizontal scale $\sqrt{U/b}$ and vertical scale $\sqrt{U/Sb}$, then the magnitude of the velocity in the baroclinic boundary current is $V = b\sqrt{S}(1-\sqrt{U/Sb})L_y$, where $L_y$ is the nondimensional distance from where $\psi = \psi_0$. For typical values of $b$ ? 1, $L_y$ ? 1, $S = O(1)$, and $U = O(1)$, $V$ ? 1 and the baroclinic boundary current is very strong compared to the interior flow. Note that the boundary current is stronger for stronger stratification, larger beta, and stronger onshore flow but it is not a simple linear dependence because both the width and depth of the boundary current depend nonlinearly on these parameters.

The upwelling into the Ekman layer is carried in a narrow region adjacent to the boundary. However, there are also significant vertical velocities forced away from the wall within the boundary current. The vertical velocity at $z$ = 0.85, derived as $w = -1/SJ(\psi, \partial\psi/\partial z)$, is shown in Fig. 5 for the region near the western boundary. There is strong upwelling over a horizontal scale of $1/\alpha$ within the region of northward flow and a symmetric downwelling in the region of southward flow. This arises as a result of the sloping isopycnals required to support the meridional flow in the baroclinic boundary current. Where the flow is to the north, the isopycnals rise towards the boundary, as required to support the thermal wind associated with the northward upper ocean velocity. Since the flow is adiabatic, the barotropic zonal flow, $U$, interacts with these sloping isopycnals to produce upwelling. The opposite happens where the meridional flow is to the south, resulting in downwelling in the boundary current. The vertical velocity forced in the baroclinic boundary current can take either sign even though the Ekman pumping in the corner is always upward.

*f. The eastward interior flow*

For steady frictionless flow, an inertial boundary layer arises as the onshore geostrophic flow impinges on the boundary. The occurrence of inertial boundary layers completely depends on the direction of the interior flow at the boundary (Greenspan, 1962; Pedlosky, 1965). We adopt an oceanic interior westward geostrophic flow towards the western boundary. However, if there were southward wind stress the interior flow would be towards the east, away from the western boundary. The potential vorticity still holds as a constant along streamlines (10a) but the sign of the last term on the left hand side is now positive. This does not support an exponentially decaying boundary current, as was found for the western boundary. Pedlosky (1965) interpreted the need for westward flow into the western boundary as a means to trap short Rossby wave energy from radiating away from the boundary. The width of the inertial boundary layer is such that the group speed of the eastward propagating Rossby waves is exactly balanced by the westward velocity *U*.

This may also be understood from consideration of the barotropic potential vorticity, defined as

$$q_{bt} = \frac{\partial v_{bt}}{\partial x} - \frac{\partial u_{bt}}{\partial y} + by = \zeta_{bt} + by \quad (18)$$

Far from the boundary, the relative vorticity $\zeta_{bt}$ is zero. At the boundary, again since the meridional scale is much larger than the zonal scale, the relative vorticity is $\partial v_{bt} / \partial x$. For northward wind stress the westward zonal interior flow impinges the western boundary and deflects either northward or southward. For northward flow, the relative vorticity in the boundary layer is negative, which can balance the increase in the planetary vorticity and vice versa for southward flow. However, for southward wind and eastward zonal interior flow, the relative vorticity in the northward flowing boundary layer will increase, as does the planetary vorticity, violating potential vorticity conservation. Therefore, the eastward flow lacks the physical mechanism to support an inertial boundary layer on the western boundary. However, as we demonstrate in the next section, a numerical model with eastward interior flow produces a boundary current very similar to that for a westward interior flow. We assert that the dissipation in the model is large enough to trap short Rossby waves near the western boundary and allow for set up of a baroclinic boundary current structure analogous to the westward interior flow cases even though the boundary current in the model is viscous, not inertial

## . Numerical Model

The quasigeostrophic theory predicts a strong baroclinic boundary current in the upper ocean whose horizontal scale is $\sqrt{U/b}$ and whose vertical scale is $\sqrt{U/Sb}$. The advantage of the inviscid, adiabatic quasigeostrophic framework is that it allows for closed form solutions and a clear interpretation of the physics that controls the structure of the boundary current. However, many strong assumptions are required which may be questionable in the near coastal region. In particular, quasigeostrophy linearizes the stratification and assumes isopycnal displacements are small. It also neglects advection of potential vorticity by the ageostrophic flow. We have neglected mixing of momentum and density, which may not be good approximations in strong, narrow surface intensified boundary currents. In this section we apply an idealized configuration of a nonlinear primitive equation model to compare with the basic predictions from the theory.

*g. Model Configuration*

The numerical model used is the MITgcm primitive equation model. The model is configured using $z$-level vertical coordinate and with a partial cell treatment of the bottom topography. This allows for accurate treatment of the pressure gradient terms in stratified flows over a sloping bottom, which is important for the present problem. The domain is 960 km by 960 km and 2000 m deep with a flat bottom and closed boundaries. The model has a uniform horizontal grid spacing of 2 km and 45 levels in the vertical with spacing ranging from 10 m over the upper 200 m to 200 m at the bottom. The initial stratification is uniform and a spatially uniform, steady, northward wind stress is applied. The model is run for a period of 120 days with the analysis taken over the final 90 days of integration. Subgridscale mixing is represented by a horizontal Smagorinsky viscosity (Smagorinsky, 1963) with nondimensional coefficient 2.5 and vertical viscosity and diffusion with coefficients $10^{-4}$ and $10^{-6}$, respectively. Additional calculations have shown that the basic results are not sensitive to these parameters. The Coriolis parameter at the southern limit of the domain is $3\times10^{-5}$ s$^{-1}$ with meridional variation $\beta = 2\times10^{-11}$ m$^{-1}$ s$^{-1}$. The wind stress for the example case is $\tau = 0.005$ N m$^{-2}$. This weak wind stress was chosen to provide a central case that would produce moderate strength currents so as to be consistent with the quasigeostrophic approximation in the theory. Stronger wind stresses, up to $0.05$ N m$^{-2}$ , are applied in the following section. The initial stratification $N^2 = 2.25\times10^{-6}$ s$^{-2}$ was chosen to give a baroclinic deformation radius of 100 km. After this central case is discussed, a series of model runs are carried out in which $\beta$, $N^2$, and $\tau$ are all varied and the results are compared with predictions from the theory in the previous section.

The inertial boundary layer width varies between 2 km and 10 km for these model runs. The Smagorinsky viscosity parameterization produces viscosities of O(10-50) m$^2$/s, which gives a viscous boundary layer width of O(10 km). This is as wide or wider than the inertial boundary layer, so that friction is important in all cases and the model western boundary layer is not purely inertial.

*Central Case*

A vertical section of the mean meridional velocity and density, averaged in time and between latitudes $y$ = 200 km and $y$ = 400 km, is shown in Fig. 6. Note that this is only the upper 1000 m and westernmost 100 km of the basin. The flow is dominated by a northward surface intensified current and a weaker southward current below. The northward flow is a maximum just off the western boundary while the southward flow is a maximum on the boundary. The interior flow towards the boundary is $O\left(10^{-4}\ \mathrm{m\,s^{-1}}\right)$, so the boundary current is approximately two orders of magnitude stronger, consistent with the theory. The horizontal scale of the boundary current is $O(10\ \mathrm{km})$, an order of magnitude less than the baroclinic deformation radius. The isopycnals are flat in the interior but they are deflected within a few kilometers of the western boundary. In the upper 50 m the isopycnals rise, providing anomalously dense water near the boundary and a horizontal density gradient to support the surface intensified jet. Over the deeper half of the countercurrent the isopycnals are deflected downward, as required to balance the local maximum in southward flow. It is clear that near the surface the quasigeostrophic assumption of spatially uniform stratification is not well satisfied, yet the basic baroclinic current structure predicted by the theory is found in the model.

There are differences between the model and the theory. Notably, the theory predicts that the countercurrent projects all the way to the surface in an ever narrowing region along the western boundary. Its absence in the numerical model is not surprising, however, because the Ekman upwelling is not confined to a delta function in the corner and the model has lateral viscosity and diffusivity that will erode such a narrow flow. The weak deep southward flow expected from the theory is also not apparent but we find that the deep flow is time-dependent as a result of basin modes that are excited by the forcing. They are sufficiently strong to alias the deep flow depending on what time period is chosen for averaging (but the stronger baroclinic flow in the upper ocean is not strongly affected). Friction is sufficiently small that they decay over a longer time scale than the model integration time. Longer time integrations result in instabilities of the western boundary current and further mask the basic current structure. Moreover, it is worth noting that there is a limitation on the applicability of our theory due to the offshore advection of density caused by Ekman transport in the surface layer. Absent a balancing surface heat flux, this will spread dense water offshore and result in convective mixing near the surface (Spall and Schneider, 2016). Therefore, we focus on the early time mean vertical structure of the upper ocean baroclinic flow in the following diagnostics.

*h. Vertical scale*

The dimensional vertical scale of the baroclinic flow was predicted by the theory to be

$$D = \frac{f_0}{N}\sqrt{\frac{U^*}{\beta}} = \sqrt{\frac{\tau f_0}{\rho_0 N^2 H^* \beta}} \quad (19)$$

For the central parameters used for the model run depicted in Fig. 6, D=127 m. The exponential decay scale used to diagnose the vertical scale in the previous section was found to be very sensitive and inconsistent when applied to the model output, especially for cases with very weak stratification. Instead, we use two different methods to diagnose the vertical scale from the model fields, one based on transport and one based on perturbation density near the boundary. The transport based diagnostic is the depth at which the meridional transport in the boundary current is a maximum. This effectively distinguishes the northward flowing upper boundary current from the deeper counter current. The density anomaly metric is the depth at which the density anomaly adjacent to the boundary has dropped to 50% of its maximum value at the surface. Reassuringly, these two measures give very similar results, 135 m and 115 m for this case, that are also close to the theoretical prediction. They are indicated on Fig. 6 by the solid and dashed red lines and compare well with the vertical scale of the baroclinic flow.

This is a scaling for the parameter dependence of the vertical decay scale of the baroclinic flow, so the best way to test this prediction is through a series of model calculations in which the governing parameters are varied. The same model configuration was used as for the central case but the values of $N^2$, $\beta$, and $\tau_0$ were varied in various combinations. The wind stress was varied between $0.00125\ \mathrm{N\ m^{-2}}$ and $0.05\ \mathrm{N\ m^{-2}}$, the stratification was varied such that the baroclinic deformation radius ranged between 10 km and 200 km, and $\beta$ was varied between $0.5\times10^{-11}\ \mathrm{m^{-1}\ s^{-1}}$ and $2\times10^{-11}\ \mathrm{m^{-1}\ s^{-1}}$. These values were chosen to provide a wide range of the primary scaling parameter $L_I/L_d$, which varied between 0.016 and 2 over 15 different model runs. The vertical length scale diagnosed in the model is compared to the scaling prediction in Fig. 7. The blue squares are for the transport-based diagnostic and the blue diamonds are for the density anomaly diagnostic. In general, the parameter dependence predicted by the theory is supported by the model calculations. The vertical length scale varies between about 60 m and 1000 m in the model with an approximately linear dependence on $L_I/L_d$. At very weak stratification (large vertical length scales) the scaling theory overpredicts the vertical scale slightly, but the model diagnostics become more sensitive to the detailed method in this limit.

The theory provides solutions only for cases in which the interior flow is towards the western boundary. To test the applicability of the scaling theory to downwelling favorable winds, for which the interior flow is eastward, we carried out 9 additional calculations in which the wind stress was varied between $-0.00125\ \mathrm{N\ m^{-2}}$ and $-0.05\ \mathrm{N\ m^{-2}}$ and the baroclinic deformation radius was varied between 10 km and 200 km. This produced values of $L_I/L_d$ between 0.016 and 1.0. These model runs produce a similar vertical length scale as the upwelling winds and are also in general agreement with the theory (Fig. 7, red symbols). We attribute the ability of the numerical model to represent boundary layer solutions even with eastward interior flow to the weak but finite viscous dissipation in the model**,** which is able to damp short Rossby waves before they can propagate energy into the interior (Pedlosky, 1965).

## Conclusions

The three-dimensional coastal upwelling forced by a uniform northward wind stress in a stratified ocean has been studied using analytical and numerical models. We adopt an oceanic interior westward geostrophic flow towards the western boundary, which balances the offshore Ekman transport and produces an inertial boundary layer as the onshore geostrophic flow impinges on the boundary.

The source/sink forcing supports a purely baroclinic boundary current in a narrow boundary layer with a horizontal scale $L_I = \sqrt{U/b}$, which is typically smaller than the deformation radius $L_d$. This scale is determined by the vorticity balance between the relative vorticity and planetary vorticity, which is wider for stronger wind stress or weaker planetary vorticity gradient. This baroclinic flow is surface intensified and decays downward with a nondimensional vertical scale of $L_I / L_d = \sqrt{U/Sb}$. Deeper than this the depth-independent onshore flow turns parallel to the boundary and flows meridionally in an inertial boundary layer. The vertical scale depends on the horizontal scale through the vorticity balance and is also larger for stronger wind stress or weaker planetary vorticity gradient. Stronger stratification means the more baroclinic flow is trapped near the surface, resulting in a smaller vertical scale. In contrast to the two-dimensional wind-driven coastal upwelling, the transition between the deep recirculating flow and the surface intensified flow marks the maximum depth of the source waters for the Ekman upwelling. This means that the depth of the source waters that feed Ekman upwelling is not an inherent length scale that depends only on the local stratification but instead deepens as the wind forcing strengthens, as the stratification weakens, or as the Coriolis parameter increases. Although the analytic solutions are valid only for westward interior flow, it is argued that if dissipation is sufficient to trap short Rossby waves then downwelling favorable winds and eastward interior flow can support western boundary currents analogous to those for westward interior flow. The basic current structure and vertical scale predicted by the theory was reproduced in an idealized primitive equation model for both upwelling and downwelling favorable winds over a wide range of parameter space.

Topography provides a forcing at $z = 0$ and alters the flat bottom solution through involving the stretching vorticity in the barotropic vorticity balance over the topographic length scale $1/\lambda$ but with a far smaller strength compare to the source/sink solution. The vertical structure of the particular solution depends on the topographic slope. For wide topographic slopes ($\lambda^2 < b/U$), the particular solution is a bottom intensified flow over a wider scale than the inertial boundary layer, which results in a small relative vorticity. If $\lambda^2 = b/U$, the topography shares the same scale as the inertial boundary layer and the balance is between the relative vorticity and $\beta$. For narrow topographic slopes ($\lambda^2 > b/U$), the relative vorticity produced by the topographically-induced flow is larger than the advection of planetary vorticity, which results in wave-like solutions in the vertical.

The westward interior transport was chosen to match the transport upwelled into the Ekman layer in anticipation that this westward flow provided the source waters for the upwelling, as for previous two-dimensional solutions. However, it was shown that, for typical parameters, most of the upwelling transport is supplied from a remote location by a narrow, shallow western boundary current, not from the interior flow. Yet this interior flow is required to maintain the western boundary current that feeds the Ekman layer, so they appear to be connected. We speculate that the interior flow represents an inertial recirculation akin to a Fofonoff free mode that might be driven by eddy fluxes as the end result of enstrophy minimization (Bretherton and Haidvogel, 1976).

## Acknowledgements

This research is supported in part by the China Scholarship Council (201906330102). H. G. is financially supported by the China Scholarship Council to study at WHOI for 2 years as a guest student. M.S. is supported by the National Science Foundation Grant OCE-1922538. Z. C. is supported by the 'Taishan/Aoshan' Talents program (2017ASTCPES05). It is a pleasure to acknowledge helpful comments on this research from Steven J. Lentz and Kenneth H. Brink.

## References


Allen, J. S., 1976: Some Aspects of the Forced Wave Response of Stratified Coastal Regions. *J. Phys. Oceanogr.*, **6**, 113–119, https://doi.org/10.1175/1520-0485(1976)006<0113:SAOTFW>2.0.CO;2.

Bretherton, F. P. and D. B. Haidvogel, 1976: Two-dimensional turbulence above topography. *J. Fluid. Mech.,* **78,**129-154.

Charney, J. G., 1955: The Generation of Ocean Currents by Wind. *J. Mar. Res.*, **14**, 477–498.

Choboter, P. F., D. Duke, J. P. Horton, and P. Sinz, 2011: Exact Solutions of Wind-Driven Coastal Upwelling and Downwelling over Sloping Topography. *J. Phys. Oceanogr.*, **41**, 1277–1296, https://doi.org/10.1175/2011JPO4527.1.

Choboter, P. F., R. M. Samelson, and J. S. Allen, 2005: A New Solution of a Nonlinear Model of Upwelling. *J. Phys. Oceanogr.*, **35**, 532–544, https://doi.org/10.1175/JPO2697.1.

Greenspan, H. P., 1962: A criterion for the existence on an inertial boundary layer in oceanic circulation. *Proc. Natl. Acad. Sci.*, **48**, 2034–2039, https://doi.org/10.1073/pnas.48.12.2034.

Halpern, D., 1974: Variations in the density field during coastal upwelling. *Tethys*, **6**, 363–374.

Hickey, B. M., 1998: Coastal oceanography of western North America from the tip of Baja California to Vancouver Island. *The Sea*, A. R. Robinson and K. H. Brink, Eds., *Regional Studies and Syntheses*, Vol. 11, John Wiley & Sons. 345-393.

Lentz, S. J., and D. C. Chapman, 2004: The Importance of Nonlinear Cross-Shelf Momentum Flux during Wind-Driven Coastal Upwelling*. *J. Phys. Oceanogr.*, **34**, 2444–2457, https://doi.org/10.1175/JPO2644.1.

Pedlosky, J., 1965: A Note on the Western Intensification of the Oceanic Circulation. *J. Mar. Res.*, **23**, 207-209.

Pedlosky, J., 1978: A Nonlinear Model of the Onset of Upwelling. *J. Phys. Oceanogr.*, **8**, 178–187, https://doi.org/10.1175/1520-0485(1978)008<0178:ANMOTO>2.0.CO;2.

Pedlosky, J., 2013: An Inertial Model of the Interaction of Ekman Layers and Planetary Islands. *J. Phys. Oceanogr.*, **43**, 1398–1406, https://doi.org/10.1175/JPO-D-13-028.1.

Smagorinsky, J., 1963: General circulation experiments with the primitive equations: I. The basic experiment. *Mon. Weather Rev.*, **91**, 99–164, https://doi.org/10.1175/1520-0493(1963)091<0099:GCEWTP>2.3.CO;2.

Spall, M. A., and N. Schneider, 2016: Coupled Ocean–Atmosphere Offshore Decay Scale of Cold SST Signals along Upwelling Eastern Boundaries. *J. Clim.*, **29**, 8317–8331, https://doi.org/10.1175/JCLI-D-16-0109.1.

Yoon, J. H., and S. G. H. Philander, 1982: The generation of coastal undercurrents. *J. Oceanogr. Soc. Japan*, **38**, 215–224, https://doi.org/10.1007/BF02111104.

Table 1. Parameters for the theory calculation used in Fig. 3. The sensitive calculations are based on the standard calculation, where $S = 1$, $U = 1$, $b = 100$, and $\lambda = 5$. In each calculation, only one parameter was altered.

| $S$ | $U$ | $b$ | $\lambda$ |
|---|---|---|---|
| 0.2 | 0.2 | 20 | 0 |
| 0.4 | 0.4 | 40 | 1 |
| 0.6 | 0.6 | 60 | 2 |
| 0.8 | 0.8 | 80 | 3 |
| 1 | 1 | 100 | 4 |
| 1.2 | 1.2 | 120 | 5 |
| 1.4 | 1.4 | 140 | 6 |
| 1.6 | 1.6 | 160 | 7 |
| 1.8 | 1.8 | 180 | 8 |
| 2 | 2 | 200 | 9 |

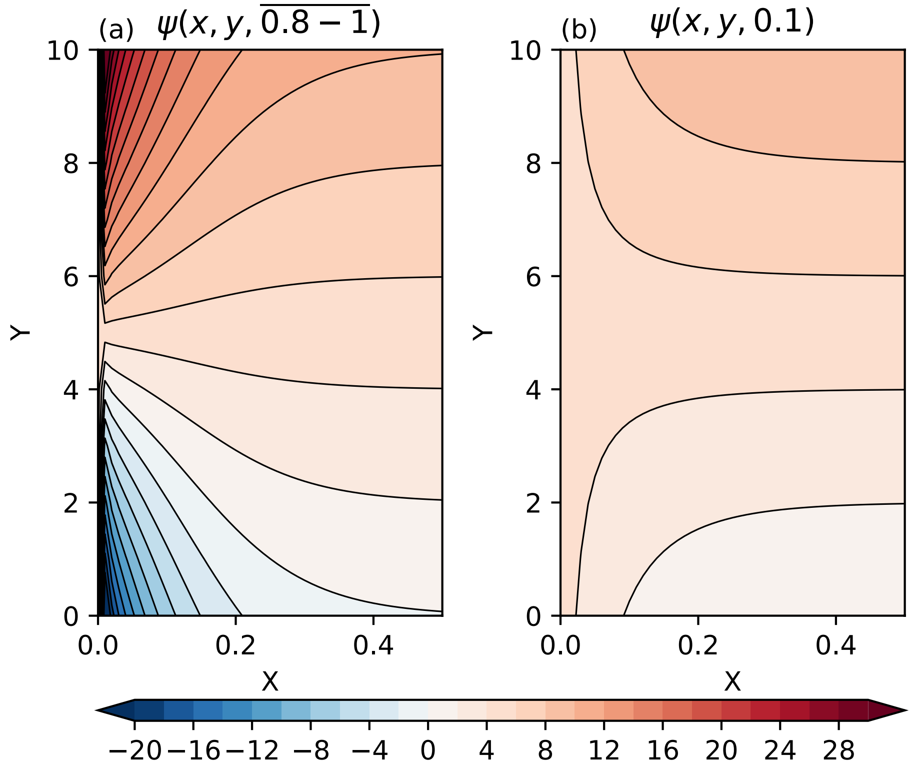


Fig. 1. The streamfunction averaged between $z$ = 0.8 and $z$ = 1 (a) and $z$ = 0.1 (b) of the source/sink solution. In this calculation $S = 1$, $b = 100$, $U = 1$, and $\psi_0 = 5$.

663

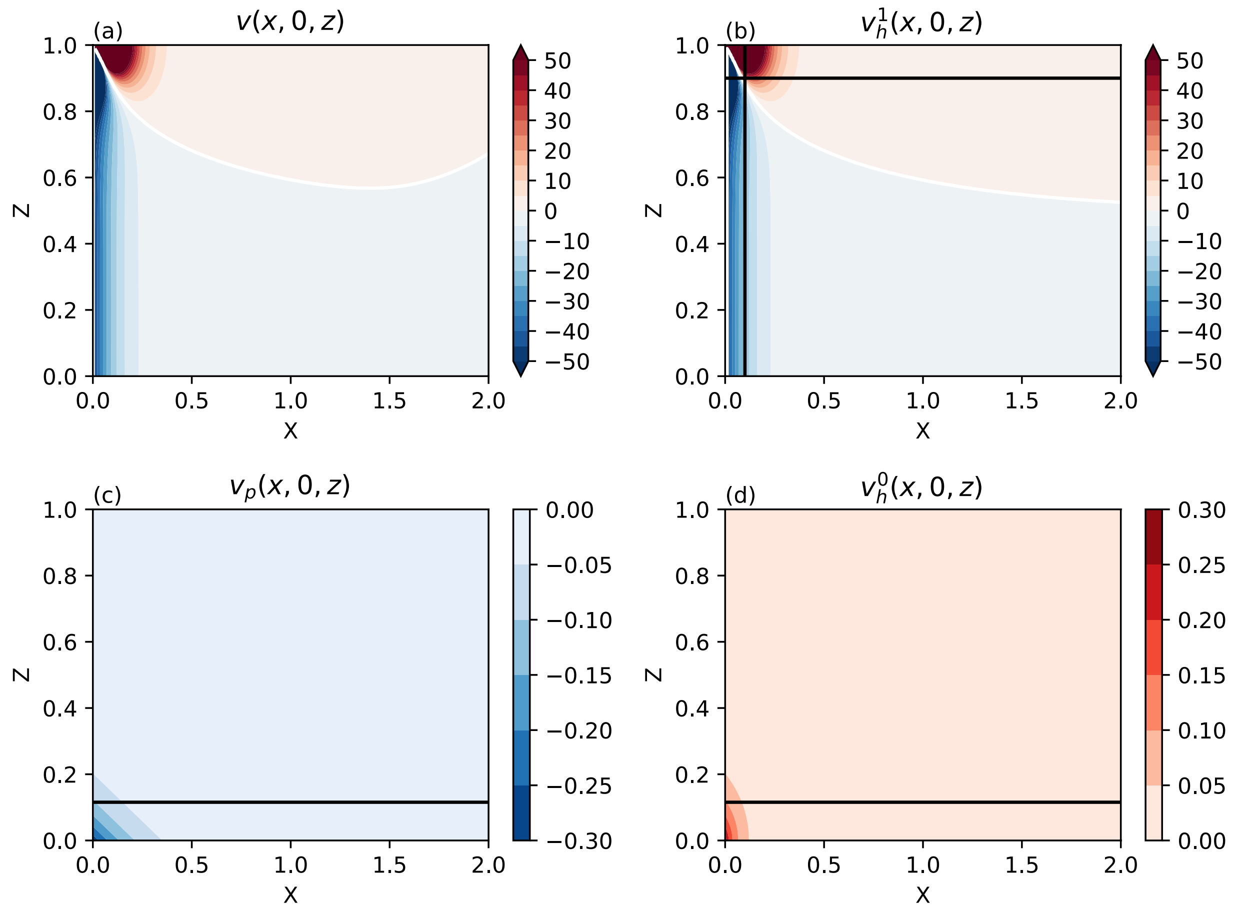


Fig. 2. Meridional velocity of the total solution (a), the source/sink forcing solution (b), the particular solution (c), and the topographic forcing solution (d) at $y = 0$. In this calculation, $S = 1$, $b = 100$, $U = 1$, $\psi_0 = 5$, $\lambda = 5$, and $h_0 = 0.5$. The black line in (c) and (d) denote the vertical scale $1/m$ in each solution, the vertical black line in (b) denotes the horizontal scale $\sqrt{U/b}$, and the horizontal black line denotes the vertical scale $\sqrt{U/Sb}$.

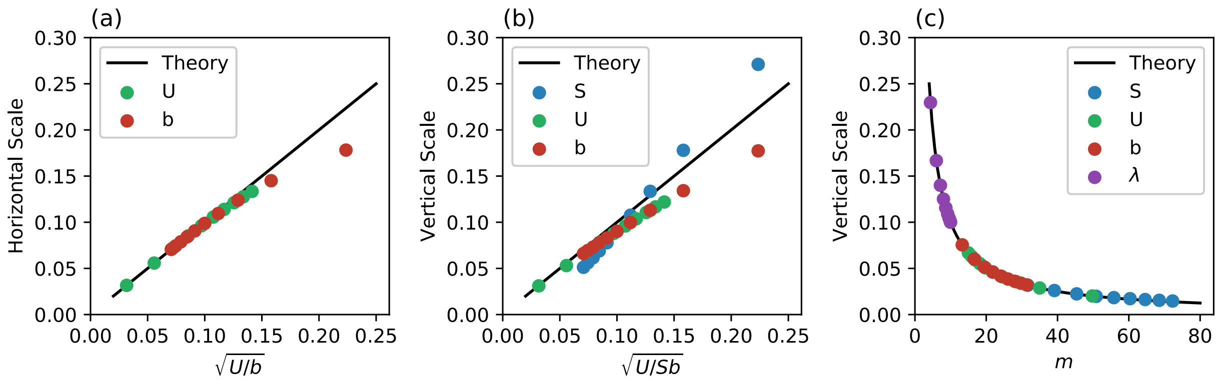


Fig. 3. Comparison between (a) the horizontal scale of the deep streamfunction at the western boundary, (b) the vertical scale of the source/sink solution at the surface, and (c) the vertical scale of the particular solution and that predicted by the scaling theory. The black line denotes the theory and the colored dots denote the scale diagnosed from the analytic solutions for a wide range of the parameters.

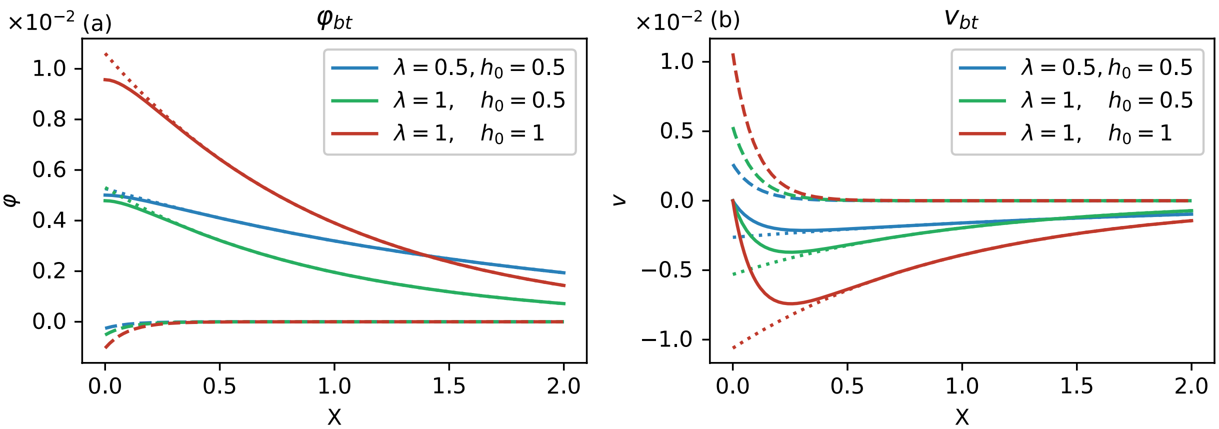


Fig. 4. (a). The barotropic perturbation streamfunction of the particular solution (dotted line) at $y$ = 0, the homogenous topographic forced solution (dashed line), and the total solutions relevant to the topography (solid line). Different colors denote the different topographic parameters. (b) As in (a) but for the barotropic meridional velocity.

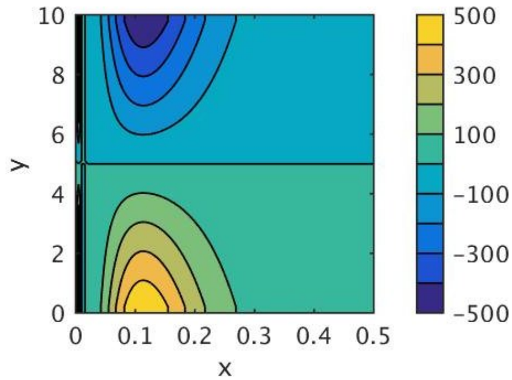


Fig. 5. Vertical velocity at $z$ = 0.85.

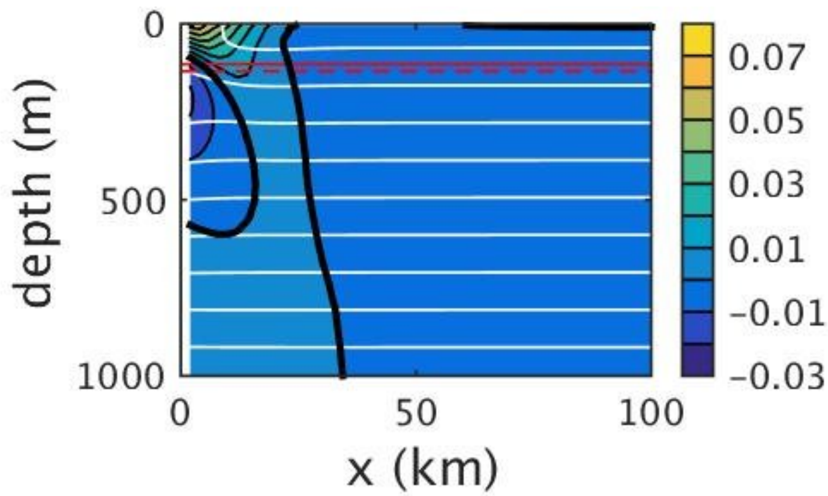


Fig. 6. Vertical section of the mean meridional velocity (colors, units m $s^{-1}$) and density field (white contours, contour interval 0.1 kg $m^{-3}$) adjacent to the western boundary, averaged between $y$ = 200 km and $y$ = 400 km. The bold black line is the zero velocity contour. The solid and dashed red lines are two measures of the vertical scale for the baroclinic flow, as described in the text.

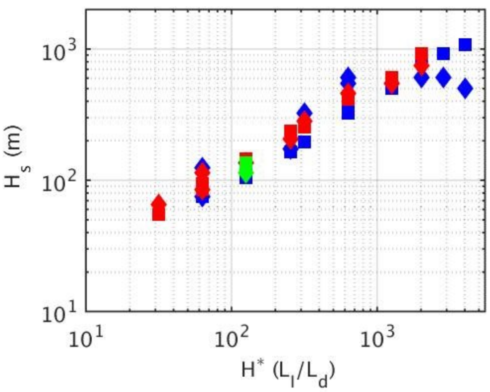


Fig. 7. A comparison between the vertical length scale diagnosed from a series of numerical model calculations ($H_s$) and the vertical scale predicted by the theory $H^*\left(L_I / L_d\right)$, where $H^* = 2000$ m is the bottom depth). The squares are derived from a transport-based diagnostic while the diamonds are based on a density anomaly metric (as described in the text). The blue symbols are for positive wind stress and the red symbols are for negative wind stress. The green symbols are for the central case discussed in Section 4.2.